Progress In Electromagnetics Research C, Vol. 121, 65–82, 2022

Bandpass-Type NGD Design Engineering and Uncertainty Analysis of RLC-Series Resonator Based Passive Cell

Yves C. Mombo Boussougou[1], Eric J. R. Sambatra[2], Antonio Jaomiary[3], Lucius Ramifidisoa[3], Nour M. Murad[4], Jean-Paterne Kouadio[5], Samuel Ngoho[5], Frank E. Sahoa[6], Sahbi Baccar[7], and Rivo Randriatsiferana[8, *]

Abstract—This paper investigates the design method, characterization, and innovative uncertainty analysis of bandpass (BP) type negative group delay (NGD) passive cell. The lumped passive topology under study consists of a resistor and a passive RLC-series network. The voltage transfer function (VTF) based circuit theory introducing the BP NGD specification analytical expressions is established in function of the R, L, and C lumped component parameters. The BP NGD performance is evaluated by figure of merit (FOM) formula. To demonstrate the BP NGD function, the design method was applied to a proof-of-concept (POC) operating at 125-kHz RFID standard center frequency. The BP NGD theory is validated by both AC simulation and measurement of POC and discrete component-based circuit prototype. Experimental BP NGD results in good agreement with calculation and simulation are obtained with NGD value of $-36.77\,\mu s$, 8% NGD bandwidth, and an attenuation lower than $-9.6\,dB$. Innovative expressions of BP NGD parameter uncertainties are established versus the POC circuit parameters. The BP NGD specification variations are interpreted with respect to the influence of constituting component uncertainties via comparison between the established NGD uncertainty theory and co-simulated sensitivity analyses.

1. INTRODUCTION

One of the open challenges expected from the modern electronic circuit designers is to deal with the signal delay effect with respect to integration density. Coupled to the undesirable noise effects, the signal delay reduces the circuit performances considerably [1–4]. Research works have been done on the electronic circuit design constraint [1–5]. A relevant model of analytical interconnect delay that accounts for the dynamic behavior of signal slope was proposed [2]. The group delay (GD) based design is useful for the improvement of certain electronic and communication devices. For example, the delay effect was exploited to enhance the gain bandwidth (BW) on negative feedback amplifiers [6]. However, adding time delay element can decrease most of the circuit performance. An alternative solution can be envisaged, for example, by using the negative group delay (NGD) function as described in the following paragraph.

Received 17 January 2022, Accepted 30 May 2022, Scheduled 30 June 2022
* Corresponding author: Rivo Randriatsiferana (rivo.randriatsiferana@univ-rennes1.fr).
[1] Université des Sciences et Techniques de Masuku (USTM), BP 901, Franceville, Gabon. [2] Institut Supérieur de Technologie D'Antsiranana (IST-D), BP 509, Antsiranana 201, Madagascar. [3] Ecole Normale Supérieure pour l'Enseignement Technique (ENSET), University of Antsiranana, BP 0, Antsiranana 201, Madagascar. [4] PIMENT, Network and Telecom Lab, Institut Universitaire de Technologie, University of La Réunion, Saint Pierre 97410, France. [5] Association Française de Science des Systèmes (AFSCET), Paris 75013, France. [6] Laboratoire de Physique Nucléaire et Physique de l'Environnement (LPNPE), Université d'Antananarivo, Antananarivo 101, Madagascar. [7] CESI Ecole d'Ingénieurs, Rouen, France. [8] Univ. Rennes, CNRS, IETR-UMR 6164, F-35000 Rennes, France.

1.1. Bibliography of NGD Electronic Circuit Potential Applications

The unfamiliar NGD function presents particular and potential applications. Literature review on NGD electronic circuit applications allows to forecast the development of innovative devices notably for RF and microwave communications engineering [7–24]. Some synthesis works of different NGD circuit applications are described in the following items:

- As intuitive application, NGD electronic circuit engineering is naturally useful to compensate and overcome the GD undesirable effect [7–10].
- A two-stage NGD planar circuit was used in a signal cancellation loop to cancel out positive DGs [11].
- Another NGD circuit (NGDC) application for designing wideband electrically small antennas by using reflection-type NGD network using open and short shunt stubs [12].
- The RF and microwave NGD circuits were employed to design some innovative non-Foster element lumped circuits [13], which represent one of the most remarkable NGD electronic circuit applications.
- An innovative design method of constant phase shifter (PS) operating independently with the frequency is introduced in [14–19]. The NGD electronic circuit-based PS can be designed by using transistor-based active, distributed and passive lumped networks [14–19].
- An innovative technique permitting to increase bandwidth of an analog feedback amplifier by employing NGDC was demonstrated in [20, 21]. As an example, the distributed element NGDC has been used to enhance a feedforward amplifier performance [21].
- And a fascinating application dedicated to electromagnetic compatibility (EMC) design engineering was recently proposed by means of resonance reduction aiming interferences cancellation [22, 23].

1.2. Brief State of the Art on Electronic Circuit NGD Design

In brief, the NGD effect was initially experimented with optical system [24–26]. Then, many interests from electronic engineering researchers were found [27–55]. Innovative microwave NGD design feasibility was verified in 2000s with left-handed metamaterial circuits [27–30]. Based on the metamaterial structure inspired designing, different NGD compact RF and microwave circuits [31–38] were proposed. Based on short-circuited coupled lines, novel topologies of reflective-type NGD networks with very small signal attenuation have been developed [32]. A distributed transmission line NGD filter was designed and implemented [33]. An innovative dual-band NGDC constituted of quarter wavelength short stubs was proposed in [34]. A design of distributed and second-order RC circuit configuration was also introduced in [35]. Some simple and efficient designs of microstrip NGDC were proposed [36–38].

In parallel with RF and microwave engineering, NGD circuit theory based on lumped element topologies was proposed [39–43]. Theoretical and experimental NGD investigations were performed with low frequency topologies [39–43]. Despite this progressive research work, the BP NGD function remains one of the most unfamiliar electronic functions for majority of current electronic design, fabrication, test and commercial engineers. Despite its counterintuitive aspect, the NGD function does not contradict the causality [39, 40]. However, because of misunderstanding and misinterpretation, the existence, design method and validation method remain open questions which need to be answered.

1.3. Fundamental Types of NGD Circuit Topologies Inspired from Filter Theory

To answer such curious questions, simpler and more fundamental circuit theory enabling to understand the different types of NGD function is necessary. An NGD circuit theory on low-pass (LP), high-pass (HP), and bandpass (BP) using NGD elementary functions was introduced [44–54]. Design approaches of LP NGD type passive circuit were proposed [44–50]. The BP NGD type approaches notably with RF and microwave topologies [27–38, 44–47, 51] are the most expanded NGD functions. In addition, uncommon characterization of other types as HP NGD function [52, 53] and stop-band NGD function [54, 55] circuits wwa recently introduced. But today, the analogy between the different types of filters and the NGD concept is still not clear enough for non-specialist electronic design and fabrication engineers.

1.4. Outline of the Paper

An RLC series resonator-based BP NGD passive topology with voltage transfer function (VTF) is presented in this paper. Innovative BP NGD experimental characterization and uncertainty analyses are introduced in the present research work, different from the active circuit S-parameter based study in [27–38, 45–47, 51]. The paper is organized into five principal sections as follows:

- Section 2 is devoted to the recall on the definitions of elementary specifications to qualify the BP NGD function.
- Section 3 develops the BP NGD theory of the considered topology. The BP NGD property of an RLC-series resonant network is described from the circuit voltage transfer function (VTF).
- Section 4 describes the feasibility study with validation results of the unfamiliar BP NGD function. The section examines the AC simulations and experimentations of proof-of-concept (POC) by designing and implementing aBP NGD circuit prototype.
- In Section 5, BP NGD circuit uncertainty analyses with respect to lumped RLC components are investigated. Then, the BP NGD specification relative variations will be discussed versus 10% tolerance of the constituting components.
- Section 6 concludes the paper.

2. BP NGD TYPE FUNCTION IDEAL SPECIFICATIONS

For the better description of the BP NGD unfamiliar aspect [27–38, 44–47, 51], we propose in this section to start with the basic function definitions. The analytical approach is based on the consideration of the VTF expression. The main frequency responses necessary for the BP NGD analysis are defined.

2.1. Representation of the Frequency Responses Necessary for the BP NGD Analysis

The BP NGD analysis [27–38, 44–47, 51] is fundamentally based on the frequency responses of the considered circuit topology VTF. For the present case of study, the circuit can be generalized by the synoptic diagram of the black box system shown in Fig. 1. Like all classical electronic circuit, the VTF can be expressed from the input and output signal voltages as represented by V_{in} and V_{out} in the diagram, respectively.

Figure 1. Ideal black box circuit.

By denoting the complex angular frequency variable, $j\omega = j2\pi f$, based on the circuit and system theory, the VTF is defined by $T(j\omega) = V_{out}(j\omega)/V_{in}(j\omega)$. The basic analytical elements to explore this response are magnitude, $T(\omega) = |T(j\omega)|$, and especially the GD defined from phase, $\varphi(\omega) = \arg[T(j\omega)]$. According to circuit theory [3–38], we can derive from this last expression the GD defined by the following definition:

$$GD(\omega) = -\frac{\partial\varphi(\omega)}{\partial\omega} \tag{1}$$

Knowing these fundamental elements, we can explore the BP NGD response. The basic characteristics of this unfamiliar function response is introduced in the following paragraph.

2.2. Definition of BP NGD Specifications

The analysis of unfamiliar BP NGD circuit topology is based on specific parameters linked to the VTF frequency responses. In this case of study, different from most of classical electronic circuit, the main parameters of the characterization are essentially the GD and magnitude. Subsequently, Fig. 2(a) and Fig. 2(b) introduce ideal plots associated with the GD and magnitude of unfamiliar BP NGD responses versus positive real frequency traditionally known as $f = \omega/(2\pi)$. As illustrated in Fig. 2(a), the GD of BP NGD ideal response should satisfy the condition: $GD(\omega_{c1} \leq \omega \leq \omega_{c2}) \approx GD_n < 0$ and $GD(\omega < \omega_{c1} \cup \omega_{c2} < \omega) > 0$. In this quantity, the term GD_n is the GD at the center frequency. Then, ω_{c1} and ω_{c2} represent the NGD cut-off frequencies.

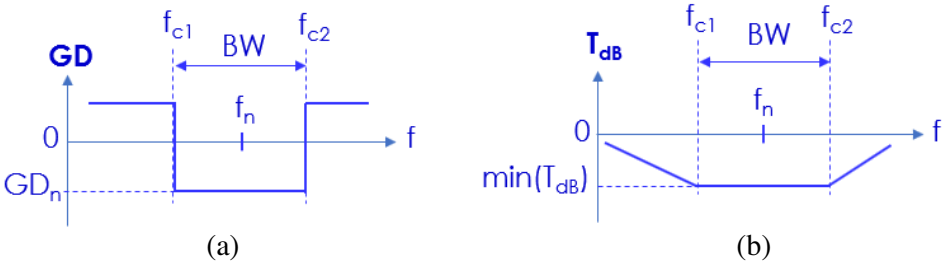

Figure 2. (a) GD and (b) magnitude of NGD ideal responses.

Following this analytical approach, we denote the NGD center frequency $\omega_n = 2\pi f_n$ and the NGD cut-off frequencies $\omega_{c,k} = 2\pi f_{c,k}$ with $k = \{1, 2\}$. These specific frequencies are related to the GD values following the mathematical equation and in equation defined by respectively $GD(\omega_{c,k}) = 0$ and $GD(\omega_n) < 0$. The NGD BW is equal to $BW_{NGD} = f_{c,2} - f_{c,1}$ which is also equal to $BW_{NGD} = (\omega_{c,2} - \omega_{c,1})/(2\pi)$. As seen in Fig. 2(b), in the frequency band $\omega_{c,1} < \omega < \omega_{c,2}$, the attenuation losses respect the classical constraints related to $T_{\min}$ as classical microwave devices $|T(j\omega)| < T_{\min}$. For more concrete investigation, let us consider, in the following section, the didactical BP NGD analysis of RLC-resonant network-based topology.

3. THEORY OF THE RLC-SERIES NETWORK BASED BP NGD TOPOLOGY

The present section develops the theoretical approach on the BP NGD analysis which will be applied to the RLC-series resonant network-based topology.

3.1. Circuit Description and VTF Expression

The considered passive cell constituting the BP NGD topology is depicted in Fig. 3. The topology under study is composed of RLC-series resonant network. To study this circuit, let us denote the impedance series $Z_n(j\omega) = R_n + j\omega L_n + 1/(j\omega C_n)$ which is composed of passive components, resistance, R_n, inductance, L_n, and capacitor, C_n. We emphasize that the BP NGD topology is different from the RLC-parallel network-based cell identified as equivalent to the split ring resonator (SRR) based left-handed metamaterial circuits as proposed in [27, 28]. The circuit is assumed fed by input voltage, V_{in}. The generated output voltage, V_{out}, is connected to shunt resistance, R.

By using the voltage divider principle, it can be demonstrated that this VTF can be rewritten explicitly in function of the RLC component values $T(j\omega) = Z_n(j\omega)/[Z_n(j\omega) + R]$. Substituting the impedance expression $Z_n(j\omega)$ into the last equation, we have:

$$T(j\omega) = \frac{R_n C_n \omega + j(L_n C_n \omega^2 - 1)}{(R + R_n) C_n \omega + j(L_n C_n \omega^2 - 1)} \tag{2}$$

Based on this VTF expression, the elaboration of frequency responses will be developed in the following subsection.

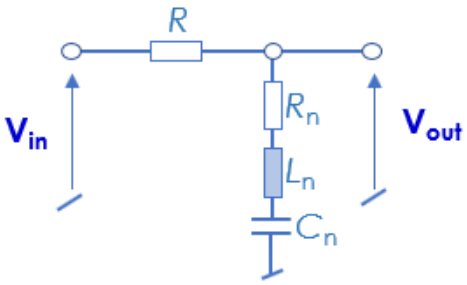

Figure 3. RLC-series network based NGD passive cell under study.

3.2. Frequency Responses of the BP NGD Topology under Study

As defined earlier in paragraph 2.1, the frequency responses considered in the present study are the magnitude, phase, and GD. By taking into account the VTF, the first one is analytically equal to:

$$T(\omega) = \sqrt{\frac{(R_n C_n \omega)^2 + (L_n C_n \omega^2 - 1)^2}{[(R + R_n) C_n \omega]^2 + (L_n C_n \omega^2 - 1)^2}} \tag{3}$$

The phase response associated to our VTF is given by:

$$\varphi(\omega) = \arctan\left(\frac{L_n C_n \omega^2 - 1}{R_n C_n \omega}\right) - \arctan\left[\frac{L_n C_n \omega^2 - 1}{(R + R_n) C_n \omega}\right] \tag{4}$$

Following the definition, the GD calculated as the derivative of the previous phase response can be written as follows:

$$GD(\omega) = \frac{(R + R_n) C_n \left(L_n C_n \omega^2 + 1\right)}{[(R + R_n) C_n \omega]^2 + (L_n C_n \omega^2 - 1)^2} - \frac{R_n C_n \left(L_n C_n \omega^2 + 1\right)}{(R_n C_n \omega)^2 + (L_n C_n \omega^2 - 1)^2} \tag{5}$$

These analytical responses will serve to establish the NGD specification parameters in function of the R, L, and C components.

3.3. Expression of BP NGD Specifications at the Resonance Frequency

The resonance angular frequency of our RLC-series network-based circuit is given by $\omega_n = 1/\sqrt{L_n C_n}$. This quantity corresponds to the following frequency $f_n = \omega_n/(2\pi)$ which can be rewritten as $f_n = 1/(2\pi\sqrt{L_n C_n})$. This frequency is assumed as the NGD center frequency in the rest of the paper. At this remarkable frequency, we have:

- The attenuation $T_n = T(\omega_n)$ becomes:

$$T_n = \sqrt{\frac{(R_n C_n \omega_n)^2}{[(R + R_n) C_n \omega_n]^2}} \tag{6}$$

  This attenuation can be simplified as:

$$T_n = \frac{R_n}{R + R_n} \tag{7}$$

- The phase is equal to $\varphi_n = \varphi(\omega_n) = 0$.
- And more importantly the fundamental formula of GD value $GD_n = GD(\omega_n)$ is:

$$GD_n = \frac{-2RL_n}{R_n (R + R_n)} \tag{8}$$

3.4. Elaboration of NGD Cut-Off Frequencies and BW

The NGD cut-off frequencies are the root of the GD established in Equation (8). After mathematical simplification, the corresponding equation is:

$$(L_nC_n)^2\omega^4 - \left[2L_nC_n + R_n\left(R + R_n\right)C_n^2\right]\omega^2 + 1 = 0 \tag{9}$$

From this equation, we determined the NGD cut-off frequencies which are expressed as:

$$f_{c1} = \frac{\sqrt{K_1 - \sqrt{K_2}}}{2\pi\sqrt{2}L_nC_n} \tag{10}$$

$$f_{c2} = \frac{\sqrt{K_1 + \sqrt{K_2}}}{2\pi\sqrt{2}L_nC_n} \tag{11}$$

where:

$$K_1 = 2L_nC_n + R_n\left(R + R_n\right)C_n^2 \tag{12}$$

$$K_2 = \left[R_n\left(R + R_n\right)C_n^2\right]^2 + 4L_nC_nR_n\left(R + R_n\right)C_n^2 \tag{13}$$

It can be analytically verified that the proposed NGD circuit presents a specific property related to the product between the two NGD cut-off frequencies:

$$f_{c1} \cdot f_{c2} = \frac{1}{\left(2\pi\right)^2 L_nC_n} \tag{14}$$

This relationship is equivalent to:

$$f_{c1} \cdot f_{c2} = f_n^2 \tag{15}$$

Another important BP NGD specification is the NGD BW defined earlier. By means of Equations (10) and (11), we have the detailed NGD BW formula, via the square $BW^2 = (f_{c2} - f_{c1})^2$ which gives:

$$BW^2 = \frac{K_1}{4\pi^2\left(L_nC_n\right)^2} - 2f_n^2 \tag{16}$$

After substitution of K_1 from equation of f_n, the previous relation can be rewritten also as:

$$BW^2 = \frac{R_n\left(R + R_n\right)C_n^2}{4\pi^2\left(L_nC_n\right)^2} \tag{17}$$

After all, we have the final NGD BW expression:

$$BW = \frac{\sqrt{R_n\left(R + R_n\right)}}{2\pi L_n} \tag{18}$$

At this stage of the study, we have theoretically demonstrated that the circuit depicted in Fig. 3 fulfills the characteristics of BP NGD function.

3.5. Analytical Investigation on BP NGD Figure of Merit (FoM)

To characterize the performance of the proposed circuit, we define the BP NGD FoM which is defined from the previous BP NGD specifications via the relation:

$$FoM = T_n \cdot |GD_n| \cdot BW \tag{19}$$

Substituting the attenuation given in Equation (7), the GD value proposed in Equation (8), and the NGD BW of Equation (18) into the previous relation, we have:

$$FoM = \frac{R_n}{\left(R + R_n\right)} \cdot \frac{2RL_n}{R_n\left(R + R_n\right)} \cdot \frac{\sqrt{R_n\left(R + R_n\right)}}{2\pi L_n} \tag{20}$$

After mathematical simplification, the later relation can be rewritten as:

$$FoM = \frac{R}{\pi\left(R + R_n\right)} \cdot \sqrt{\frac{R_n}{R + R_n}} \tag{21}$$

For the case of our NGD circuit, this FoM quantity can also be expressed in function of the attenuation by means of Equation (7). Accordingly, we have:

$$FoM = \frac{(1 - T_n) \cdot \sqrt{T_n}}{\pi} \tag{22}$$

The NGD circuit is optimized from the point of view of the NGD if and only if FoM is maximum. We can demonstrate that the derivative of this function can be expressed as:

$$\frac{d\left[FoM(T_n)\right]}{dT_n} = \frac{1 - 3T_n}{2\pi\sqrt{T_n}} \tag{23}$$

It means that the maximum of the BP NGD RLC-series circuit, FoM, is reached when:

$$\left.\frac{d\left[FoM(T_n)\right]}{dT_n}\right|_{T_n = T_{n_{opt}}} = 0. \tag{24}$$

Consequently, based on expression (23), the root of Equation (24) is $T_{n_{opt}} = 1/3$ which implies $R = 2R_n$. In this case, the BP NGD FoM is equal to $FoM_{\max} = 2/(3\pi\sqrt{3})$. Moreover, we also have the NGD value-BW product:

$$|GD_n| \cdot BW = \frac{2}{\pi\sqrt{3}} \tag{25}$$

This last relation explains that $|GD_n|$ and BW are inversely proportional for our BP NGD topology. If we choose to have a large NGDBW, $|GD_n|$ will be small and vice versa.

3.6. Synthetic Formulations of BP NGD Specifications

Table 1 recapitulates the basic expressions of the BP NGD specific parameters of the RLC-series resonant network based passive cell. It is worth to note that in the expressions exposed in Table 1, the units of resistor, inductor, and capacitor parameters are in Ohm (Ω), Henry (H), and Farad (F), respectively.

Table 1. General expression and optimized expression for main NGD parameters.

BP NGD parameters	General expressions	Optimal expressions
f_n [Hz]	$\frac{1}{2\pi\sqrt{L_n C_n}}$	-
T_n	$\frac{R_n}{R+R_n}$	$\frac{1}{3}$
GD_n [s]	$-\frac{2RL_n}{R_n(R+R_n)}$	$-\left(\frac{4}{3}\right) \cdot \frac{L_n}{R_n}$
BW [Hz]	$\frac{\sqrt{R_n(R+R_n)}}{2\pi L_n}$	$\left(\frac{\sqrt{3}}{2\pi}\right) \cdot \frac{R_n}{L_n}$
FoM	$\frac{R}{\pi(R+R_n)} \cdot \sqrt{\frac{R_n}{R+R_n}} = \frac{(1-T_n)\cdot\sqrt{T_n}}{\pi}$	$\frac{2}{3\pi\sqrt{3}}$

These formulas of second column express the BP NGD specifications under the particular case where the angular frequency $\omega = \omega_n$. Then, the third column of the table presents the values corresponding to the case of optimal BP NGD FoM. For the feasibility study of the established BP NGD engineering of the previously established theory, AC validation results with low frequency (LF) circuit are explored in the next section.

4. PRACTICAL STUDY OF THE BP NGD CIRCUIT WITH AC SIMULATION AND EXPERIMENTAL VALIDATION

For the BP NGD engineering feasibility study, the design and parameters of the circuit POC are described in the present section. The BP NGD validation in the LFs will be explored by discussion between the results from theoretical model, simulation, and experimentation.

4.1. Description of the BP NGD POC Design

Like all electronic function, the initial step of the BP NGD design engineering is the choice of the BP NGD specifications. In the next step, the parameters of RLC-series network-based circuit announced earlier in Fig. 2 must be determined. In this second step, the ideal component values constituting the circuit must be calculated. Accordingly, we propose to consider the frequency band specification corresponding to RFID standard with 125 kHz center frequency. Therefore, the desired BP NGD specifications indicated in the first row of Table 2 are considered. As use case of the POC, based on the established theory of Section 3, the R, R_n, L_n, and C_n parameters of the BP NGD passive cell introduced in Fig. 3 were calculated.

Table 2. BP NGD desired specifications and circuit parameters.

Objective	Description	Name	Value
Desired BP NGD specifications	Center frequency	f_n	125 kHz
	Attenuation	T_n	1/3
	BW	BW	115 kHz to 135 kHz
	NGD value	GD_n	-36.77 µs
POC circuit parameters	Resistor	R	725.2 Ω
		R_n	362.6 Ω
	Inductor	L_n	10 mH
	Capacitor	C_n	162 pF

Table 3. Characteristics of the tested components constituting the BP NGD circuit demonstrator.

Name	Quantity	Designation	Nominal value	Manufacturer references	Tolerance
Resistor	2	R	680 Ω + 47 Ω	Reference: 892-6070 and 892-5581 at RS seller©/Carbon Film Resistor	Serie E24 (5% relative inaccuracy)
	2	R_n	330 Ω + 33 Ω	Reference: 892-5575 and 892-5409 at RS seller©/Carbon Film Resistor	Serie E24 (5% relative inaccuracy)
Inductor	1	L_n	10 mH	Reference: 800-4381 at RS seller©/Radial inductance, Resonance frequency 1 kHz, 23.8 Ω R_{dc}	Serie E12 (10% relative inaccuracy)
Capacitor	2	C_n	150 pF + 10 pF	Reference: 892-6070 and 892-5581 at RS seller©/Carbon Film Capacitor	Serie E6 (20% relative inaccuracy)

The second row of Table 2 summarizes the obtained values of the BP NGD circuit POC considered in the present study. Table 3 addressed the list of the components employed to build the BP NGD CUT. Two components were interconnected in parallel to realize the resistances, R and R_n. The same two capacitors were interconnected in parallel to realize the capacitor, C. The relative tolerances of the resistors, inductor, and capacitor are classified in series E24, E12, and E6, respectively. To validate the

calculated model, based on the previously determined and chosen nominal parameters, the BP NGD circuit was designed and simulated. One underlines that LF AC simulations were carried out by the ADS® commercial tool from Keysight Technologies®. This software tool is dedicated to the electrical and electronic circuit simulation. Fig. 4 represents the design of the BP NGD RLC-series network-based circuit POC in the ADS® schematic environment.

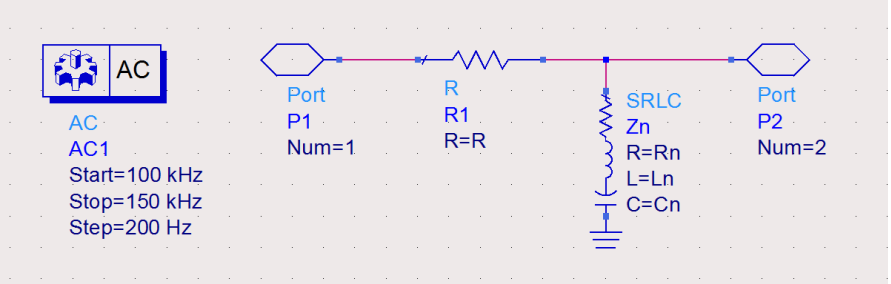

Figure 4. ADS® design of the simulated BP NGD circuit.

The simulations were performed in AC regime with minimal frequency, $f_{\min} = 100\,\text{kHz}$, and maximal frequency, $f_{\max} = 150\,\text{kHz}$, over 250 frequency samples. To validate the BP NGD aspect experimentally, the POC was experimentally investigated. The implemented and experimented validation results will be examined in the following reminder of the paper. The innovative technique of the BP NGD experimental setup will be described in the next paragraph.

4.2. Description of the BP NGD Experimental Setup

An experimentation technique of BP NGD aspect in the LFs was realized to validate the BP NGD function practically with the proposed RLC-series circuit. The present subsection will describe how the measurement was realized, and the data processing was performed. As a matter of fact, Fig. 5(a) illustrates the performed BP NGD experimental setup. This innovative practical study was made by measurements of harmonic sine signals by sweeping the period or frequency. During the test, the input

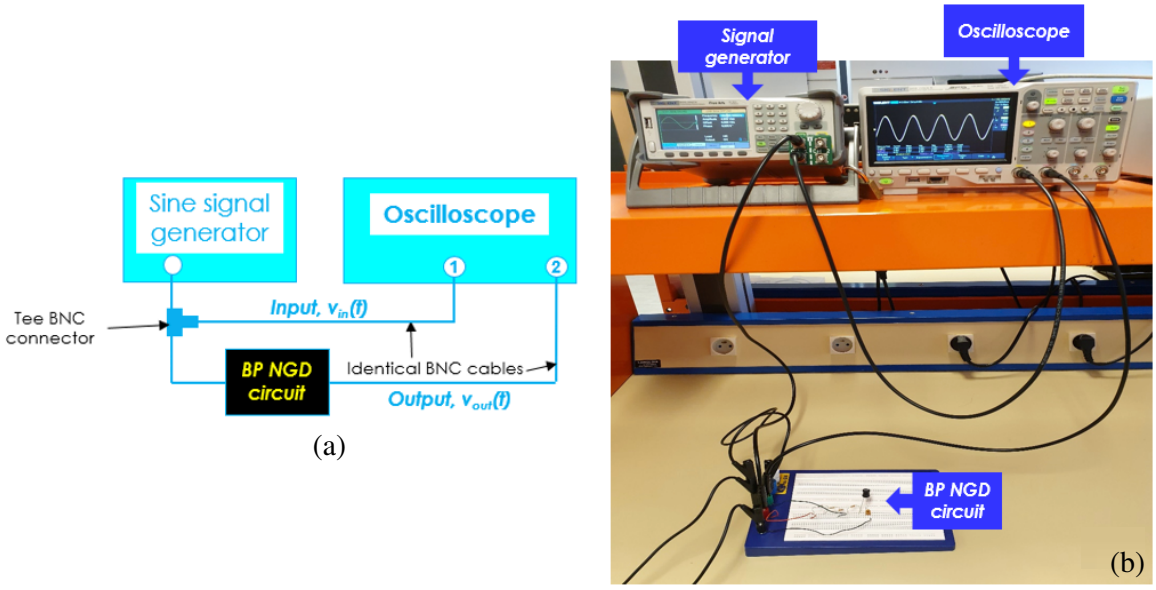

Figure 5. (a) Illustrative diagram and (b) photograph of the performed BP NGD experimental setup.

signal is injected from the LF signal generator (SIGLENT SDG 2042X) with possibility of frequency tuning in the operating band of interest. Then, the RLC-series circuit prototype was mounted on the solderless breadboard. The LF signal generator and the oscilloscope (SIGLENT SDS 1104X-E) were interconnected to the circuit under test (CUT) via BNC cables as illustrated in Fig. 5(b). With such a setup, we may wonder how the frequency responses are established. The next paragraph will answer this query with the analytical description of measured data post-processing.

4.3. Measured Data Post-Processing

The amplitudes and phase shifts defined by the t-time dependent analytically are expressed as:

$$v_{in}(t) = A_{\max}\sin(2\pi ft) \tag{26}$$

$$v_{out}(t) = B_{\max}\sin(2\pi ft + \Delta\varphi) \tag{27}$$

with input signal amplitude, $A_{\max}$, which is fixed to 1 V, output signal amplitude, $B_{\max}$, and input-output phase shift, $\Delta\varphi$. The test frequency, f, was sampled as f_k, with k varied from 1 to maximal index:

$$k_{\max} = Ent\left[\frac{f_{\max} - f_{\min}}{\Delta f}\right] \tag{28}$$

with the $Ent[\cdot]$ being the superior integer part function. The magnitude and phase of measured VTF are extracted from equation, respectively:

$$T_{\text{measured}}(f_k) = \frac{B_{\max}(f_k)}{A_{\max}(f_k)} \tag{29}$$

$$\varphi_{\text{measured}}(f_k) = \Delta\varphi(f_k) \tag{30}$$

with $f_k = k\Delta f$ varied from $f_{\min} = f_1$ and $f_{\max} = f_{k_{\max}}$. By incrementing k from 2 to $k_{\max}$, the measured GD is determined for the later equation by the relation corresponding to the discretization of Equation (1):

$$GD_{\text{measured}}(f_k) = \frac{\varphi_{\text{measured}}(f_k) - \varphi_{\text{measured}}(f_{k-1})}{2\pi(f_k - f_{k-1})} \tag{31}$$

To verify the effectiveness of the proposed experimental work, discussion between the calculated, simulated and measured results will be presented.

4.4. Calculated, Simulated and Experimental Validation Results

To validate the BP NGD behavior, theoretical calculation with MATLAB®, simulation from ADS®, and measurement results are discussed in the present subsection. The measurement was carried out by sweeping the sine frequency f of the input signal expressed in Equation (26) from minimal frequency $f_{\min} = 150\,\text{kHz}$ to maximal frequency $f_{\max} = 250\,\text{kHz}$ step $\Delta f = 5\,\text{kHz}$. The input sine test signal was windowed over the time width, $T_{\max} = 40\,\mu\text{s}$. After recording the amplitudes and phase shift between the input and output sine signals, the NGD circuit responses were determined from Equations (29), (30), and (31). The comparisons of the curves representing the calculated ("solid navy-blue line"), simulated ("dashed blue-sky line"), and measured ("dotted red line"), frequency responses of the POC of RLC-series circuit are plotted in Fig. 6. We emphasize that the magnitudes, phases, and GDs shown in Fig. 6(a), Fig. 6(b), and Fig. 6(c), respectively, are in excellent agreement. The GDs of Fig. 6(c) confirm that the proposed lumped passive topology behaves as a BP NGD function. The notable difference between the calculation and measurement is mainly due to the employed component tolerances, the measurement systematic errors by using the BNC cables and connectors, and also the employed LF generator and oscilloscope imperfections. Nevertheless, the calculation and simulation differences are literally negligible in the whole test frequency band. Furthermore, the NGD phenomenon appears theoretically at the NGD center frequency with NGD value of about $GD_n = -37\,\mu\text{s}$ over the NGD BW, $BW_n = 10\,\text{kHz}$ as expected in Table 2.

In other words, this BW corresponds to about 8% of the NGD center frequency. The RLC-series circuit attenuation is about 9.54 dB at the NGD center frequency. For an oversee about the comparative study between the validation results, uncertainty analyses of the different parameters specifying the NGD function will be explored in the next section.

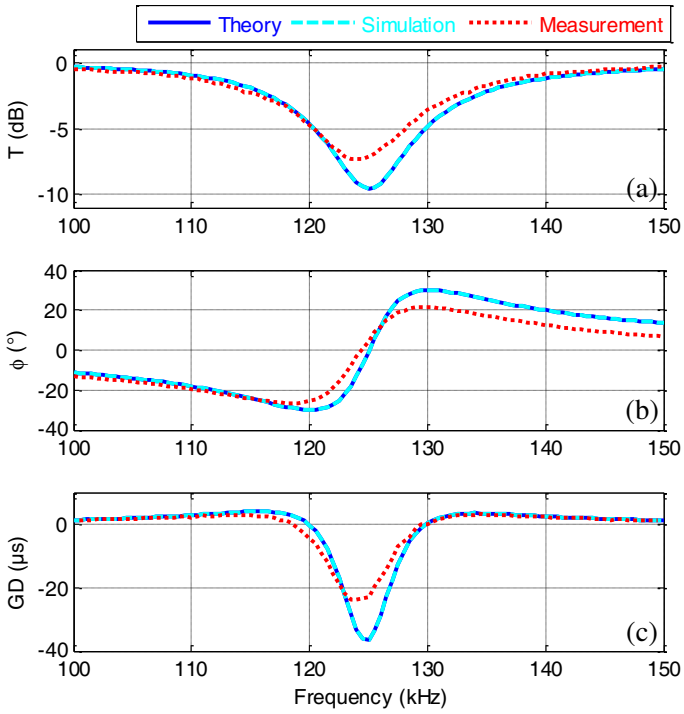

Figure 6. Calculated, simulated and measured responses: (a) magnitude, (b) phase and (c) GD.

5. UNCERTAINTY INVESTIGATION VERSUS R, L, AND C COMPONENT TOLERANCES

Acting as an unfamiliar function, it would be important to perform an error analysis illustrating the relevance of the considered BP NGD passive cell. The uncertainty study of the BP NGD response never being done before is investigated in the present section. After parametric analyses, the theoretical expressions and computed error results are discussed. Then, the uncertainty investigation will be discussed in function of the used R, L, and C component tolerances.

5.1. Mapping Plots of BP NGD Frequency Responses with RLC Parameter Influences

This subsection deals with the study of the R, R_n, L_n, and C_n parameter variations on the BP NGD circuit frequency responses. The parametric study is based on the mapping of magnitude, phase, and GD frequency responses by taking into account of the lumped parameters. The ADS parametric AC simulations were run with $\pm 10\%$ tolerance variations around the nominal values of each component. It can be seen in Figs. 7(a) and 7(b) that the resistances substantially affect all the BP NGD specifications. The BP NGD circuit VTF magnitude varies with R_n while increasing R causes it to decrease further. In the same way, the band of variation of T generated by R_n seems more important than that caused by R. The NGD BW undergoes variations but almost equal for the two parameters. The BP NGD cell is therefore sensitive to resistances but a little more so with R_n. These impacts are similarly reflected in the phase and GD. We find that R_n reduces the BW much more than R. On the other hand, R_n allows for more delay, especially for its small values. Figs. 8(a) and 8(b) show the influences of reactive components L_n and C_n, respectively. As forecasted by formula (22), the two quantities influence the NGD central frequency similarly.

We can see in both Figs. 8(a) and 8(b) that their increase causes the decrease of the NGD central frequency through a trajectory in elliptical form. The reactive component variations do not affect the VTF magnitude of the BP NGD circuit neither in optimal value nor in BW aperture. However, C_n seems to have more impact on the level of variation of the GD. These parametric analyses lead us to characterize the uncertainty of the BP NGD specifications versus the lumped elements.

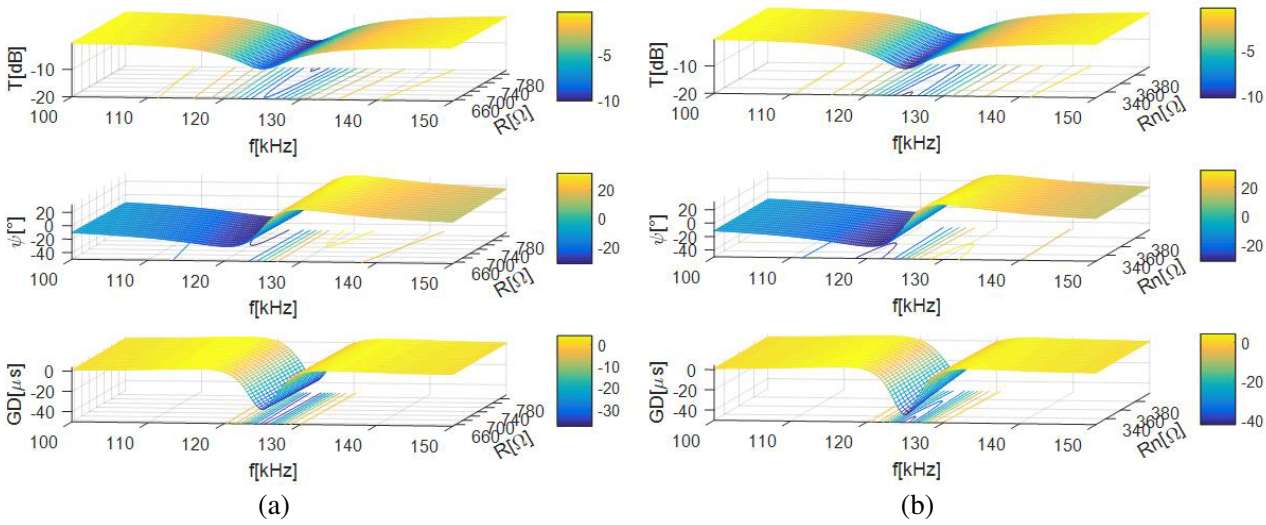

Figure 7. Mapping plots of magnitude, phase and GD versus resistors (a) R and (b) R_n, and frequency.

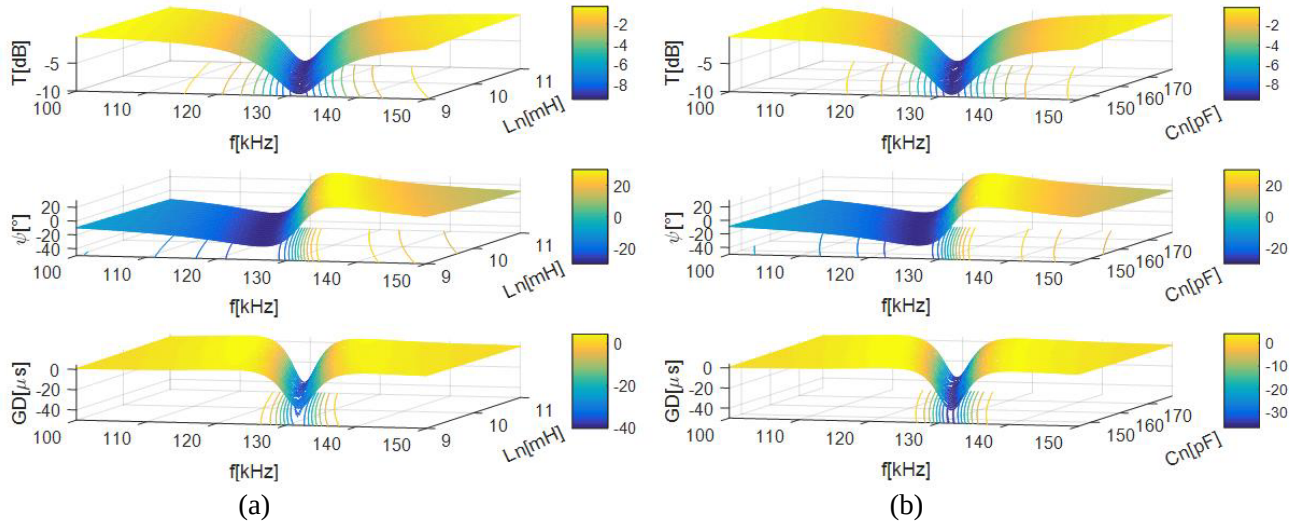

Figure 8. Mapping plots of magnitude, phase and GD versus (a) L_n and (b) C_n, and frequency.

5.2. BP NGD Specification Uncertainty Theoretical Analyses

We recall that the theoretical expressions of the uncertainties are established from the multivariate function, $y(x_1, x_2, ..., x_m)$ (with m being a positive integer) differentiation:

$$dy(x_1, x_2, ..., x_m) = \sum_{k=1}^{m} \frac{\partial y}{\partial x_k} dx_k \tag{32}$$

The absolute uncertainty is established substituting dx_k by Δx_k, dy by Δy, and the partial derivative $\partial y/\partial x_k$ by $|\partial y/\partial x_k|$. Consequently, Equation (50) becomes:

$$\Delta y = \sum_{k=1}^{m} \left| \frac{\partial y}{\partial x_k} \right| \Delta x_k \tag{33}$$

Based on this discretization definition, we establish the theoretical expressions of the NGD specification uncertainties with respect to the NGD circuit parameters, R, R_n, L_n, and C_n. It implies that the

relative errors corresponding to the uncertainties of NGD center frequency f_n, attenuation expressed in Equation (7), GD value established in Equation (8), and also the NGD BW elaborated in Equation (18) are respectively:

$$\frac{\Delta f_n}{f_n} = \frac{1}{2} \cdot \left(\frac{\Delta L_n}{L_n} + \frac{\Delta C_n}{C_n} \right) \tag{34}$$

$$\frac{\Delta T_n}{T_n} = \left(\frac{R}{R+R_n} \right) \cdot \left(\frac{\Delta R}{R} + \frac{\Delta R_n}{R_n} \right) \tag{35}$$

$$\frac{\Delta GD_n}{GD_n} = \left(\frac{R_n}{R+R_n} \right) \cdot \frac{\Delta R}{R} + \left(\frac{R+2R_n}{R+R_n} \right) \cdot \frac{\Delta R_n}{R_n} + \frac{\Delta L_n}{L_n} \tag{36}$$

$$\frac{\Delta BW}{BW} = \frac{1}{2} \cdot \left(\frac{R}{R+R_n} \right) \cdot \frac{\Delta R}{R} + \frac{1}{2} \cdot \left(\frac{R+2R_n}{R+R_n} \right) \cdot \frac{\Delta R_n}{R_n} + \frac{\Delta L_n}{L_n} \tag{37}$$

Under a similar way, we have the NGD FoM uncertainty established earlier in Equation (22) from the formula:

$$\frac{\Delta FoM}{FoM} = \frac{1}{2} \cdot \left(\frac{R+2R_n}{R+R_n} \right) \cdot \left(\frac{\Delta R}{R} + \frac{\Delta R_n}{R_n} \right) \tag{38}$$

Based on these formulations, the variations of NP NGD specifications were computed in function of the passive elements R, R_n, L_n, and C_n. And the computed results are compared with the ADS® AC simulations.

5.3. Simulated BP NGD Characteristic Variations

Based on ADS® parametric AC simulations, we can verify the consistence of the previously established uncertainty formulas by considering the ±10% variations of passive elements around the nominal values. The main specifications were generated from the mapping computations in the previous subsection. The

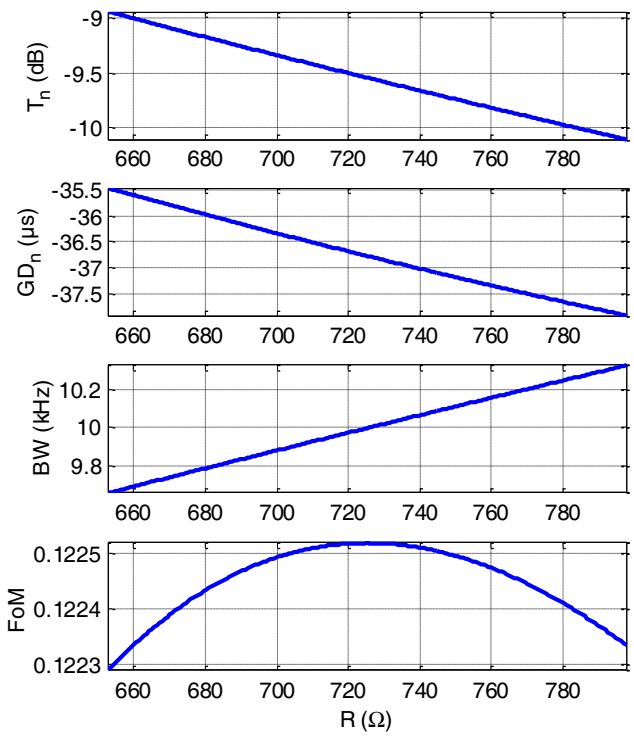

Figure 9. Attenuation, NGD value, NGD BW and BP NGD FoM versus R.

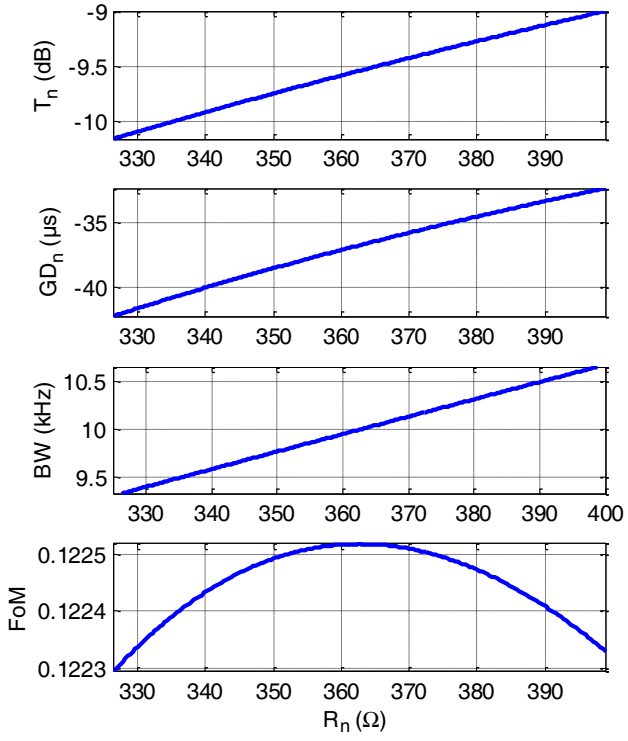

Figure 10. Attenuation, NGD value, NGD BW and BP NGD FoM versus R_n.

obtained BP NGD specification results of R, R_n, L_n, and C_n variations are displayed Figs. 9, 10, and 11, respectively. We can remark that except the BP NGD FoM, all variations of T_n, GD_n, and BW around the central frequency are linear. These three last specifications increase with R_n, contrary to the effect of L_n. The increase of R decreases T_n when it could act in favor of GD_n and BW. According to Equations (7) and (22), the attenuation at the NGD center frequency and the FoM do not depend on L_n and C_n, and they are about $T_n \approx -9.54\,\text{dB}$ and $FoM \approx 0.122$. This justifies their constant appearance in Fig. 11. Finally, we observe in Figs. 9 and 10 that FoM reaches its optimal value at the nominal values of R and R_n. It should be pointed out that these two values were initially chosen for optimal operation. Their decreases/increases lead to quasi-symmetrical decreases of FoM around the central frequency. These variations are relatively small because the $\pm 10\%$ of variations considered at the level of R and R_n would result in less than 0.17% of variation of FoM_n.

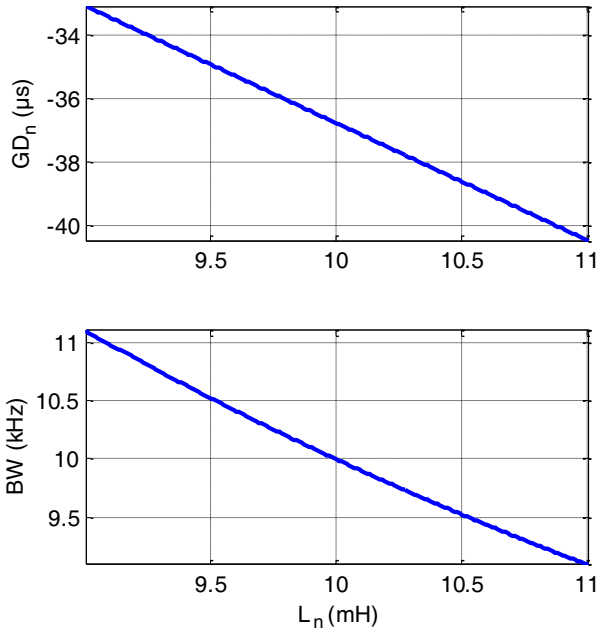

Figure 11. Attenuation, NGD value and NGD BW versus L_n.

5.4. Uncertainty Numerical Results of BP NGD Characteristics

The theoretical uncertainties were calculated by considering the theoretical values of R, L, and C elements of Table 3 via Equations (34) to (38). As a matter of fact, we obtain the numerical results of Table 4 which summarizes the uncertainty and relative errors of NGD center frequency, attenuation, GD value, NGD BW, and BP NGD FoM from the theory and measurement. The uncertainty analyses

Table 4. Calculated uncertainties and relative errors between theory and measurement.

Parameters	Theoretical values	Theoretical Uncertainties	Measured values	Theory-measured relative errors
f_n	125 kHz	7.5%	124.5	0.4%
T_n	0.33	6.7%	0.43	30%
GD_n	$-36.77\,\mu$s	18.33%	-23.3	36%
BW	10 kHz	15%	11	10%
FoM_n	0.12	6.7%	0.11	8.3%

are based on the component tolerances in series E12. It can be pointed out that the measured values of the circuit parameters are close to the theoretical values except for the gain and the GD which are outside the expected intervals.

6. CONCLUSION

A BP NGD theoretical and experimental study of lumped RLC-series network based passive cell is investigated. The BP NGD engineering research work proposes innovative uncertainty analyses and LF characterization technique never done before. The theoretical analysis is established in function of the BP NGD topology lumped components. The BP NGD circuit design method is elaborated with a POC expected to originally operate around the RFID frequency band. The BP NGD parameter uncertainty variations versus the circuit components ones with respect to their tolerances are expressed to find the optimal components values according to the given specifications.

To validate the BP NGD design method, an LF circuit POC model is simulated, fabricated, and measured. Measurement results in good agreement with the model and simulation confirm the BP NGD behavior. The discrepancies between simulation and measurement are commented with the respect to the employed lumped component tolerances and systematic measurement errors. The uncertainty analyses were presented with innovative formulas of relative inaccuracies of each BP NGD parameter and comparison with schematic AC co-simulation including parametric analyses.

In the continuation of the present research work, further study taking into account the R, L, and C parasitic effects of realistic components which are susceptible to modify the NGD parameters will be developed.

REFERENCES

1. Kang, S.-M. and H. Y. Chen, "A global delay model for domino CMOS circuits with application to transistor sizing," *International Journal of Circuit Theory and Applications*, Vol. 18, No. 3, 289–306, 1990.
2. Hwang, M.-E., S.-O. Jung, and K. Roy, "Slope interconnect effort: Gate-interconnect interdependent delay modeling for early CMOS circuit simulation," *IEEE Transactions on Circuits and Systems I: Regular Papers*, Vol. 56, No. 7, 1428–1441, 2008.
3. Groenewold, G., "Noise and group delay in active filters," *IEEE Transactions on Circuits and Systems I: Regular Papers*, Vol. 54, No. 7, 1471–1480, 2007.
4. Myoung, S.-S., B.-S. Kwon, Y.-H. Kim, and J.-G. Yook, "Effect of group delay in RF BPF on impulse radio systems," *IEICE Transactions on Communications*, Vol. 90, No. 12, 3514–3522, 2007.
5. Ravelo, B., "Delay modeling of high-speed distributed interconnect for the signal integrity prediction," *The European Physical Journal Applied Physics*, Vol. 57, No. 3, 31002, 2012.
6. Alves, L. N. and R. L. Aguiar, "A time-delay technique to improve GBW on negative feedback amplifiers," *International Journal of Circuit Theory and Applications*, Vol. 36, No. 4, 375–386, 2008.
7. Ahn, K.-P., R. Ishikawa, and K. Honjo, "Group delay equalized UWB InGaP/GaAs HBT MMIC amplifier using negative group delay circuits," *IEEE Trans. Microw. Theory Techn.*, Vol. 57, No. 9, 2139–2147, 2009.
8. Ravelo, B., S. Lalléchère, A. Thakur, A. Saini, and P. Thakur, "Theory and circuit modeling of baseband and modulated signal delay compensations with low-and band-pass NGD effects," *AEU-Int. J. Electronics Communications*, Vol. 70, No. 9, 1122–1127, 2016.
9. Shao, T., Z. Wang, S. Fang, H. Liu, and Z. N. Chen, "A group-delay-compensation admittance inverter for full-passband self-equalization of linear-phase band-pass filter," *AEU-Int. J. Electronics Communications*, Vol. 123, 153297–153309, 2020.

10. Xiao, J.-K., Q.-F. Wang and J.-G. Ma, "Negative group delay circuits and applications: Feedforward amplifiers, phased-array antennas, constant phase shifters, non-foster elements, interconnection equalization, and power dividers," *IEEE Microwave Magazine*, Vol. 22, No. 2, 16–32, Feb. 2021.
11. Jeong, Y., H. Choi, and C. D. Kim, "Experimental verification for time advancement of negative group delay in RF electronic circuits," *Electronics Letters*, Vol. 46, No. 4, 306307, 2010.
12. Almahroug, A. A., B. M. Amer, Z. H. M. Fheleboom, S. Rehan, and A. I. A. Omer, "Designing a reflection-type NGD network using open and short shunt stubs for wideband electrically small antennas," *Journal of Applied Science*, Vol. 1, No. 6, 61–75, Apr. 2021.
13. Zhang, T., R. Xu, and C.-T. M. Wu, "Unconditionally stable non-foster element using active transversal-filter-based negative group delay circuit," *IEEE Microwave and Wireless Components Letters*, Vol. 27, No. 10, 921–923, 2017.
14. Ravelo, B., M. Le Roy, and A. Perennec, "Application of negative group delay active circuits to the design of broadband and constant phase shifters," *Microwave and Optical Technology Letters*, Vol. 50, No. 12, 3077–3080, Dec. 2008.
15. Ravelo, B., A. Perennec, and M. Le Roy, "Synthesis of frequency-independent phase shifters using negative group delay active circuit," *Int. J. RFMiCAE*, Vol. 21, No. 1, 17–24, Jan. 2011.
16. Ravelo, B., G. Fontgalland, H. S. Silva, J. Nebhen, W. Rahajandraibe, M. Guerin, G. Chan, and F. Wan, "Original application of stop-band negative group delay microwave passive circuit for two-step stair phase shifter designing," *IEEE Access*, Vol. 10, No. 1, 1493–1508, 2022.
17. Ravelo, B., "Distributed NGD active circuit for RF-microwave communication," *Int. J. Electronics Communications*, Vol. 68, No. 4, 282–290, Apr. 2014.
18. Nebhen, J. and B. Ravelo, "Innovative microwave design of frequency-independent passive phase shifter with LCL-network and bandpass NGD circuit," *Progress In Electromagnetics Research C*, Vol. 109, 187–203, 2021.
19. Ravelo, B., G. Fontgalland, H. S. Silva, J. Nebhen, W. Rahajandraibe, M. Guerin, G. Chan, and F. Wan, "Original application of stop-band negative group delay microwave passive circuit for two-step stair phase shifter designing," *IEEE Access*, Vol. 10, No. 1, 1493–1508, 2022.
20. Choi, H., Y. Jeong, C. D. Kim, and J. S. Kenney, "Bandwidth enhancement of an analog feedback amplifier by employing a negative group delay circuit," *Progress In Electromagnetics Research*, Vol. 105, 253–272, 2010.
21. Choi, H., Y. Jeong, C. D. Kim, and J. S. Kenney, "Efficiency enhancement of feedforward amplifiers by employing a negative group-delay circuit," *IEEE Trans. Microw. Theory Techn.*, Vol. 58, No. 5, 1116–1125, 2010.
22. Ravelo, B., F. Wan, J. Nebhen, W. Rahajandraibe, and S. Lalléchère, "Resonance effect reduction with bandpass negative group delay fully passive function," *IEEE Transactions on Circuits and Systems II: Express Briefs*, Vol. 68, No. 7, 2364–2368, Jul. 2021.
23. Ravelo, B., S. Lalléchère, W. Rahajandraibe, and F. Wan, "Electromagnetic cavity resonance equalization with bandpass negative group delay," *IEEE Transactions on Electromagnetic Compatibility*, Vol. 63, No. 4, 1248–1257, Aug. 2021.
24. Segard, B. and B. Macke, "Observation of negative velocity pulse propagation," *Physics Letters A*, Vol. 109, No. 5, 213–216, 1985.
25. Macke, B. and B. Ségard, "Propagation of light-pulses at a negative group-velocity," *The European Physical Journal D — Atomic, Molecular, Optical and Plasma Physics*, Vol. 23, No. 1, 125–141, 2003.
26. Bukhman, N. S., "On the principle of causality and superluminal signal propagation velocities," *Journal of Communications Technology and Electronics*, Vol. 66, 227–241, 2021.
27. Eleftheriades, G. V., O. Siddiqui, and A. K. Iyer, "Transmission line models for negative refractive index media and associated implementations without excess resonators," *IEEE Microwave and Wireless Components Letters*, Vol. 13, No. 2, 51–53, 2003.

28. Siddiqui, O. F., M. Mojahedi, and G. V. Eleftheriades, "Periodically loaded transmission line with effective negative refractive index and negative group velocity," *IEEE Trans. Antennas and Propagation*, Vol. 51, No. 10, 2619–2625, 2003.
29. Monti, G. and L. Tarricone, "Negative group velocity in a split ring resonator-coupled microstrip line," *Progress In Electromagnetics Research*, Vol. 94, 33–47, 2009.
30. Markley, L. and G. V. Eleftheriades, "Quad-band negative-refractive-index transmission-line unit cell with reduced group delay," *Electronics Letters*, Vol. 46, No. 17, 1206–1208, 2010.
31. Liu, G. and J. Xu, "Compact transmission-type negative group delay circuit with low attenuation," *Electronics Letters*, Vol. 53, No. 7, 476–478, Feb. 2017.
32. Chaudhary, G. and Y. Jeong, "Low signal-attenuation negative group-delay network topologies using coupled lines," *IEEE Trans. Microw. Theory Techn.*, Vol. 62, No. 10, 2316–2324, 2014.
33. Chaudhary, G., Y. Jeong, and J. Lim, "Microstrip line negative group delay filters for microwave circuits," *IEEE Trans. Microw. Theory Techn.*, Vol. 62, No. 2, 234–243, 2014.
34. Choi, H., Y. Jeong, J. Lim, S.-Y. Eom, and Y.-B. Jung, "A novel design for a dual-band negative group delay circuit," *IEEE Microwave Wireless Components Letters*, Vol. 21, No. 1, 19–21, 2010.
35. Ahn, K.-P., R. Ishikawa, A. Saitou, and K. Honjo, "Synthesis for negative group delay circuits using distributed and second-order RC circuit configurations," *IEICE Trans. Electronics*, Vol. 92, No. 9, 1176–1181, 2009.
36. Ravelo, B., "Negative group-delay phenomenon analysis with distributed parallel interconnect line," *IEEE Transactions on Electromagnetic Compatibility*, Vol. 58, No. 2, 573–580, Apr. 2016.
37. Ravelo, B., "Theory on coupled line coupler-based negative group delay microwave circuit," *IEEE Trans. Microw. Theory Techn.*, Vol. 64, No. 11, 3604–3611, Nov. 2016.
38. Ravelo, B., "Innovative theory on multiband negative group delay topology based on feedback loop power combiner," *IEEE Transactions on Circuits and Systems II: Express Briefs*, Vol. 63, No. 8, 738–742, Aug. 2016.
39. Mitchell, M. W. and R. Y. Chiao, "Causality and negative group delays in a simple bandpass amplifier," *American Journal of Physics*, Vol. 66, No. 1, 14–19, 1998.
40. Mitchell, M. W. and R. Y. Chiao, "Negative group delay and "fronts" in a causal system: An experiment with very low frequency bandpass amplifiers," *Physics Letters A*, Vol. 230, Nos. 3–4, 133–138, 1997.
41. Nakanishi, T., K. Sugiyama, and M. Kitano, "Demonstration of negative group delays in a simple electronic circuit," *American Journal of Physics*, Vol. 70, No. 11, 1117–1121, 2002.
42. Kitano, M., T. Nakanishi, and K. Sugiyama, "Negative group delay and superluminal propagation: An electronic circuit approach," *IEEE J. Selected Topics in Quantum Electronics*, Vol. 9, No. 1, 43–51, 2003.
43. Munday, J. N. and R. H. Henderson, "Superluminal time advance of a complex audio signal," *Applied Physics Letters*, Vol. 85, No. 3, 503–505, 2004.
44. Ravelo, B., "Similitude between the NGD function and filter gain behaviours," *International Journal of Circuit Theory and Applications*, Vol. 42, No. 10, 1016–1032, 2014.
45. Ravelo, B., "On the low-pass, high-pass, bandpass and stop-band NGD RF passive circuits," *URSI Radio Science Bulletin*, Vol. 2017, No. 363, 10–27, Dec. 2017.
46. Yuan, A., S. Fang, Z. Wang, H. Liu, and H. Zhang, "A novel band-stop filter with band-pass, high-pass, and low-pass negative group delay characteristics," *Hindawi Int. J. Antennas and Propagation*, Vol. 2021, Article ID 3207652, 1–15, 2021.
47. Yuan, A., S. Fang, Z. Wang, and H. Liu, "A novel multifunctional negative group delay circuit for realizing band-pass, high-pass and low-pass," *Electronics*, Vol. 10, No. 1742, 1–12, 2021.
48. Ravelo, B., "First-order low-pass negative group delay passive topology," *Electronics Letters*, Vol. 52, No. 2, 124–126, Jan. 2016.
49. Randriatsiferana, R., Y. Gan, F. Wan, W. Rahajandraibe, R. Vauché, N. M. Murad, and B. Ravelo, "Study and experimentation of a 6-dB attenuation low-pass NGD circuit," *Analog. Integr. Circ. Sig. Process.*, 1–14, Apr. 2021.

50. Wan, F., N. Li, B. Ravelo, Q. Ji, B. Li, and J. Ge, "The design method of the active negative group delay circuits based on a microwave amplifier and an RL-series network," *IEEE Access*, Vol. 6, 33849–33858, 2018.
51. Ngoho, S., Y. C. Mombo Boussougou, S. S. Yazdani, Y. Dong, N. M. Murad, S. Lalléchère, W. Rahajandraibe, and B. Ravelo, "Design and modelling of ladder-shape topology generating bandpass NGD function," *Progress In Electromagnetics Research C*, Vol. 115, 145–160, 2021.
52. Wan, F., X. Huang, K. Gorshkov, B. Tishchuk, X. Hu, G. Chan, F. E. Sahoa, S. Baccar, M. Guerin, W. Rahajandraibe, and B. Ravelo, "High-pass NGD characterization of resistive-inductive network based low-frequency circuit," *COMPEL — The International Journal for Computation and Mathematics in Electrical and Electronic Engineering*, Vol. 40, No. 5, 1032–1049, 2021.
53. Yang, R., X. Zhou, S. Yazdani, E. Sambatra, F. Wan, S. Lalléchère, and B. Ravelo, "Analysis, design and experimentation of high-pass negative group delay lumped circuit," *Circuit World*, 1–25, Aug. 2021.
54. Fenni, S., F. Haddad, K. Gorshkov, B. Tishchuk, A. Jaomiary, F. Marty, G. Chan, M. Guerin, W. Rahajandraibe, and B. Ravelo, "AC low-frequency characterization of stop-band negative group delay circuit," *Progress In Electromagnetics Research C*, Vol. 115, 261–276, 2021.
55. Guerin, M., Y. Liu, A. Douyère, G. Chan, F. Wan, S. Lalléchère, W. Rahajandraibe, and B. Ravelo, "Design and synthesis of inductorless passive cell operating as stop-band negative group delay function," *IEEE Access*, Vol. 9, No. 1, 100141–100153, Jul. 2021.